Title
LEASTIC SCATTEEING OF CHEMICALLY REACTIVE MOLECULES

Authors
Herschbach, Dudley R.
Kwei, George H.

Publication Date
1963-08-01

UCRL-11178

University of California

Ernest O. Lawrence Radiation Laboratory

ELASTIC SCATTERING OF CHEMICALLY REACTIVE MOLECULES

Berkeley, California

DISCLAIMER

3rd. International Conference on
Collision Processes - Amsterdam
June 1963

UCRL-11178

UNIVERSITY OF CALIFORNIA

Lawrence Radiation Laboratory
Berkeley, California

AEC Contract No. W-7405-eng-48

ELASTIC SCATTERING OF CHEMICALLY REACTIVE MOLECULES

Dudley R. Herschbach and George H. Kwei

August, 1963

ELASTIC SCATTERING OF CHEMICALLY REACTIVE MOLECULES*

D. R. Herschbach† and G. H. Kwei†‡

Department of Chemistry and Lawrence Radiation Laboratory, University of California, Berkeley, California

Abstract

The angular distribution and the velocity dependence of the total elastic scattering cross section are calculated for a potential which presents a deep "chemical well" at small distances and a van der Waals well at large distances. A two-body central force model and semiclassical mechanics are used. It is found that the chemical well suppresses much of the wide angle scattering and under suitable conditions may introduce several special effects, including "multiple rainbows" and "chemical orbiting" in the angular distribution and "beats" in the undulatory velocity dependence of the total cross section.

---

*Support received from the U. S. Atomic Energy Commission and the Alfred P. Sloan Foundation is gratefully acknowledged.

An abbreviated version of this report is to be published in Proceedings of the Third International Conference on the Physics of Electronic and Atomic Collisions, London (North-Holland Publishing Company, Amsterdam, 1963).

†Present address: Department of Chemistry, Harvard University, Cambridge, Massachusetts.

‡Woodrow Wilson Foundation Predoctoral Fellow, 1961-63.

Most collisions of potentially reactive molecules do not lead to reaction but to elastic or inelastic scattering. However, the nonreactive and the reactive modes of scattering are usually governed by the same potential energy surface, since most chemical reactions are "electronically adiabatic" and the lowest potential surface ordinarily lies far below those for higher electronic states. The distribution in angle and energy of the product molecules depends upon both the entrance and the exit valley of the potential surface, whereas practically all the molecules scattered without reaction have sampled only the entrance valley. Thus we may expect that often the nonreactive scattering will offer more direct information about the initial conditions which favor reaction than can be obtained from studies of reactive scattering.

For exothermic reactions without appreciable activation energy, the entrance valley presents an extended downhill slope through part of the region that would comprise the repulsive core in collisions of molecules that cannot react. The primary effect of this "softness" of the potential should be to suppress much of the wide angle elastic scattering that would appear for a potential of the Lennard-Jones type. The small angle scattering should be little affected, as it is almost solely determined by the long-range behavior of the potential.

A marked fall-off in the elastic scattering at large angles has been observed in molecular beam studies of several reactive systems.[1-4] This has

previously been attributed to depletion by reaction and analyzed on the assumption that otherwise the wide angle scattering could be predicted from a Lennard-Jones or Exp-6 potential chosen to fit the small angle scattering. However, for the five examples which have been studied, this interpretation is found to imply a reaction cross section from 5 to 50 times larger than that estimated from direct measurement of the product distribution.

In order to evaluate the fall-off in wide angle scattering and other qualitative features which might prove useful for the experimental characterization of the entrance valley in the potential surface, we have calculated the angular distribution and the velocity dependence of the total scattering cross section for several potentials which may be appropriate to various types of reactions. This paper describes the results obtained for one of the simplest possibilities, a potential with an outer van der Waals well that blends monotonically into an inner chemical well, and also considers briefly some aspects of the scattering from related types of two-well potentials.

TWO-BODY MODEL

We shall treat the elastic scattering of reactive molecules as a two-body central force problem. This is, of course, a drastic idealization. However, the experimental data available at present can give only a qualitative picture of the potential, and in view of our ignorance of chemical interactions the results would remain almost equally speculative even if a rigorous treatment of the mechanics were feasible. Also, as indicated below, it can be plausibly argued that if solutions to the actual multidimensional

problem were available, the comparison with experiment would essentially involve a pre-averaging over vibrational coordinates and a post-averaging over rotational coordinates. Under ordinary conditions the result is likely to be practically equivalent to the use of a fictitious central force potential.

This approach is very similar to the "optical potential" or "cloudy crystal ball" model popular in nuclear physics.[5] In molecular scattering, however, it should be possible to relate the fictitious central force potential derived from a two-body analysis of the experimental scattering data to properties of the actual multidimensional potential surface. We hope eventually to carry out a detailed examination of this aspect of the optical potential approach to inelastic molecular collisions; here we shall consider only the most rudimentaly features.

In the scattering of an atom A by a diatomic molecule BC, the actual potential is three dimensional, $V(\xi,\alpha,r)$, a function of the translational coordinate r (distance from A to center of mass of BC), the vibrational coordinate ξ of the BC molecule, and the angle α between the vectors $\underset{\sim}{r}$, and $\underset{\sim}{\xi}$. A rough idea of the dependence of the potential on r and ξ may be obtained from van der Waals parameters and vibrational frequencies, as illustrated in Figs. 1-3 for the K + HBr example. The relevant parameters are given in Table I, in terms of the customary notation.[6] The van der Waals parameters for K + HBr correspond to the Exp-6, α = 12 potential[6] which Beck employed in analyzing his scattering experiments.[1,7] This potential is plotted in Fig. 1(a). There is as yet no experimental information on the van der Waals parameters for KBr + H. The estimates given in Table I were obtained as follows: σ was taken as the sum of the van der Waals radii for

hydrogen (1.2 Å) and bromine (1.95 Å) atoms as given by Pauling;[8] r_m was obtained from $r_m = 1.1225\sigma$, the relation which holds for a Lennard-Jones potential[6]; and ε was taken as the experimental value[9] for Kr + Li, which might be expected to be a rough upper limit for the Br + H interaction. The vibrational potential parameters for the HBr molecule were obtained from Herzberg's compilation;[10] those for KBr from more recent experimental results.[11,12,13] The harmonic oscillator vibrational potentials plotted in Fig. 1(b) are obtained from

$$V(\xi)/\hbar\omega_e = 0.01483\ m\omega_e(\Delta\xi)^2$$

where $V(\xi)$ and $h\omega_e$ are in kcal/mole, m is the reduced mass of the molecule in g/mole, ω_e the vibrational frequency in cm^{-1}, and $\Delta\xi$ the displacement from the equilibrium bond distance in Å units.

Fig. 2 shows a contour map for the HBr + K → KBr + H reaction. This was constructed by using the parameters of Table I to plot the separate potential wells (shown by dashed contours) which would obtain for the reactants and products if there were no chemical interaction but only van der Waals interactions, and then smoothly interpolating (solid contour lines) between these wells. The activation energy was assumed to be negligible. Thus, since the classical dissociation energies D_e (measured from the potential minimum) are virtually identical, the canyon which connects the reactant and product valleys has an almost flat floor and sides which flare out rapidly in the transition from the narrow HBr + K valley to the broad KBr + H valley.

The portion of the potential surface which governs the thermal energy nonreactive scattering of HBr + K is shown in a magnified view in Fig. 3. Since the H atom is so light, the translational coordinate r is essentially the Br - K distance; the vibrational coordinate ξ is the H - Br distance. Again the

Table I. Potential parameters for the K + HBr → KBr + H system.

	Translational potentials			
	ε kcal/mole	r_m Å	σ Å	$C = 2\varepsilon r_m^6$ 10^{-60} erg cm^6
r(K - HBr)	0.55	4.9	4.35	1035
r'(KBr - H)	0.18	3.5	3.15	47

	Vibrational potentials			
	D_o^o kcal/mole	D_e kcal/mole	ω_e kcal/mole cm^{-1}	r_e Å
ξ(HBr)	86.4	90.2	7.57 2650	1.412
ξ'(KBr)	90.2	90.5	0.61 213	2.821

The asymptotic form of the translational potential is $V(r) = -C/r^6$, where $C = 0.139\ \varepsilon r_m^6$, with C in units of 10^{-60} erg cm^6, ε in kcal/mole, and r_m in Å.

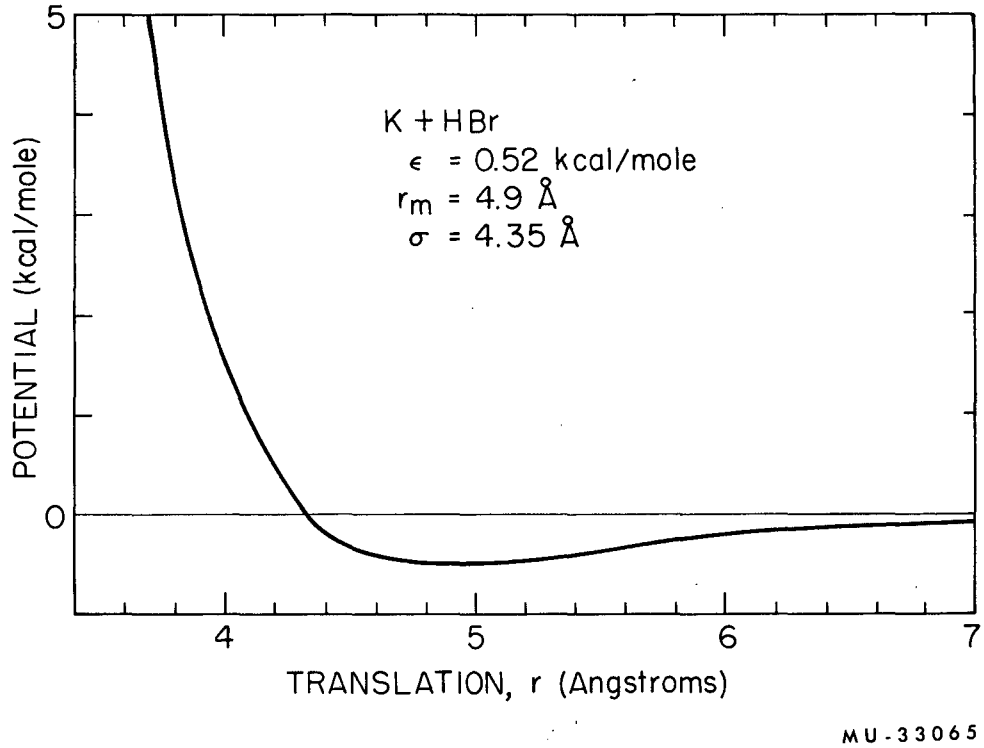
5
0
POTENTIAL (kcal/mole)
K + HBr
ϵ = 0.52 kcal/mole
r_m = 4.9 Å
σ = 4.35 Å
4
5
6
7
TRANSLATION, r (Angstroms)
MU-33065

Fig. 1a

Fig. 1b

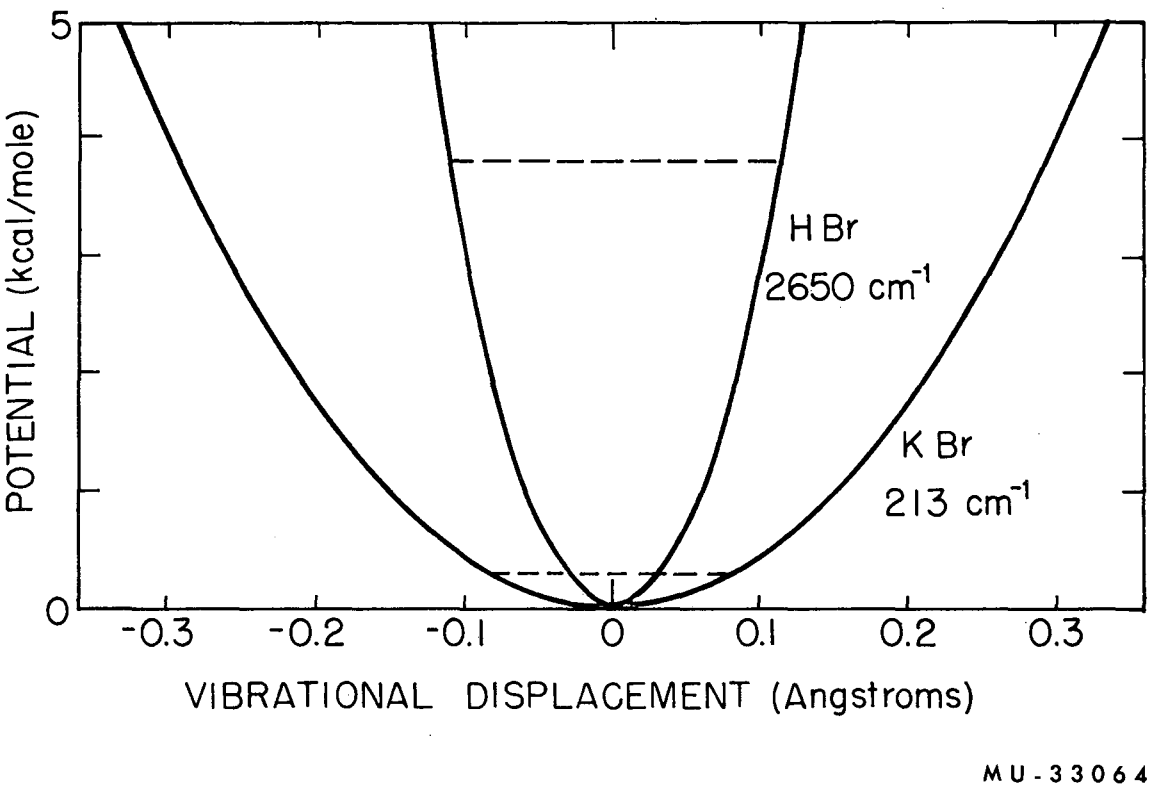
5
0
POTENTIAL (kcal/mole)
H Br
2650 cm^{-1}
K Br
213 cm^{-1}
-0.3
-0.2
-0.1
0
0.1
0.2
0.3
VIBRATIONAL DISPLACEMENT (Angstroms)
MU-33064

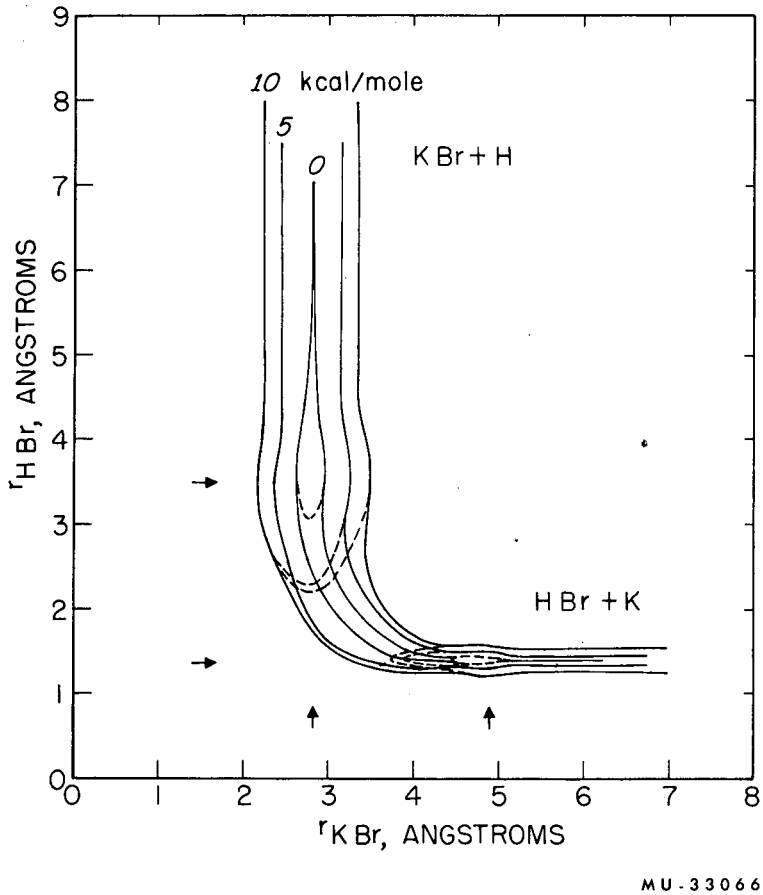
10 kcal/mole
5
0
K Br + H
H Br + K
$r_{H\,Br}$, ANGSTROMS
$r_{K\,Br}$, ANGSTROMS
0
1
2
3
4
5
6
7
8
9
MU-33066

Fig. 2

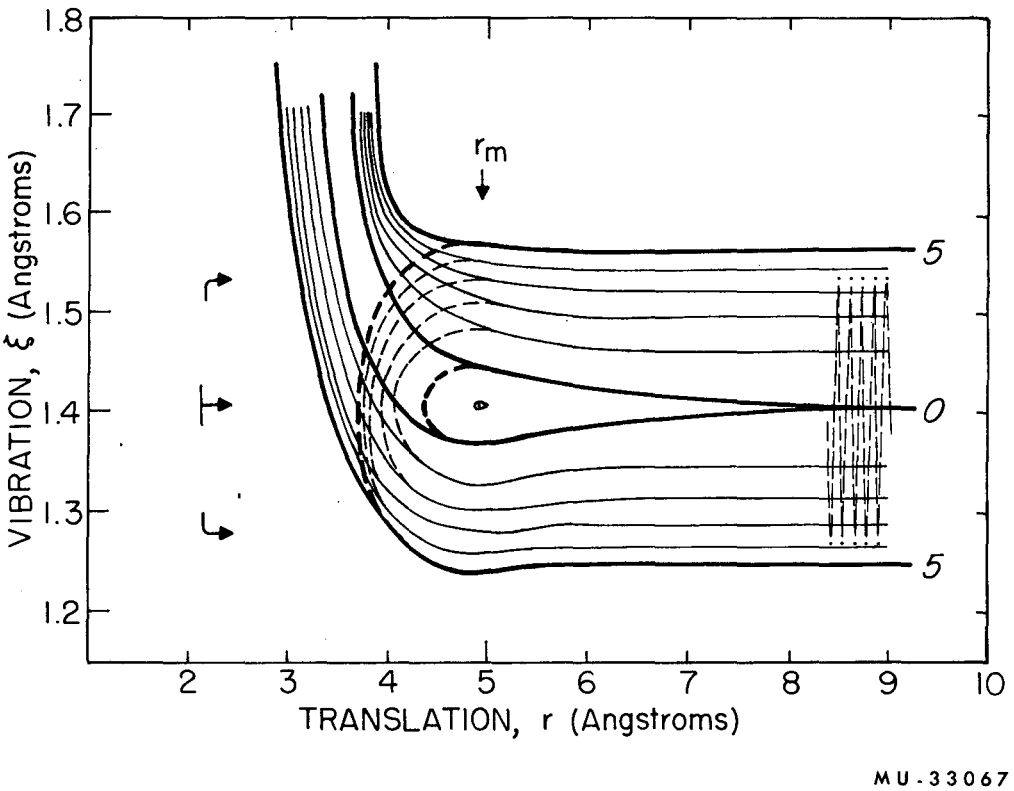
1.8
1.7
1.6
1.5
1.4
1.3
1.2
VIBRATION, ξ (Angstroms)
2
3
4
5
6
7
8
9
10
TRANSLATION, r (Angstroms)
r_m
5
0
5
MU-33067

Fig. 3

dashed contours give the potential which would obtain if only the van der Waals interaction were present. The repulsive wall of Fig. 1(a) is seen to be considerably displaced and tilted backwards by the chemical interaction. As already noted, we expect this to account for the most important qualitative differences in the elastic scattering of reactive and nonreactive molecules.

Approximate Separability of Vibration

In the region $r > r_m$, the vibrational motion in ξ is much more rapid than the translational and rotational motions and therefore is practically separable. For the sample trajectory shown on the right side of Fig. 3, the initial translational relative velocity is 10^5 cm/sec, and thus the representative point travels 1 Å along the r-direction in 10^{-13} sec; there are meanwhile about 8 cycles of the ξ-vibration, however, since the zero-point vibrational period of HBr is only 0.126×10^{-13} sec. A procedure analogous to the Born-Oppenheimer approximation employed in molecular spectroscopy[14,15] then yields an effective Hamiltonian

$$\hat{H}_{TR} = \hat{T}(r,\alpha) + V(r,\alpha), \tag{1a}$$

which corresponds to an average of the complete Hamiltonian over the rapid vibrational motions. The kinetic energy operator $\hat{T}(r,\alpha)$ includes the original translational terms, the rotational kinetic energy of a rigid HBr molecule, and various coupling terms. The effective potential energy is given by

$$V(r,\alpha) = \int V(\xi,\alpha,r)\,|\psi_\xi(\xi,\alpha,r)|^2 d\xi \tag{1b}$$

where ψ_ξ is the vibrational wavefunction evaluated for fixed values of α and r; the weighting factor thus varies parametrically with α and r, since the frequency of the transverse ξ-vibrations varies somewhat along the entrance valley of the potential surface, and there is also some perturbation via vibration-rotation

coupling.[15] For collisions of nonreactive molecules (dashed contours in Fig. 3), Eqs. (1) also hold to a good approximation in the region $r < r_m$, although the weighting factor $|\psi_\xi|^2$ varies rapidly with r near the repulsive wall, and additional terms omitted from the Hamiltonian (1a) become large enough to induce transitions between vibrational states.[16]

For elastic collisions of reactive molecules Eqs. (1) will become progressively poorer approximations the deeper the trajectories penetrate within $r < r_m$. In this region, however, the optimum choice of coordinates corresponds to "mixing" r and ξ to give again a low frequency translational coordinate r^* (which more or less parallels the equipotential curves in Fig. 3) and a high frequency vibrational coordinate ξ^* (approximately transverse to the equipotentials). In transition state theory,[17] r^* is termed the "reaction coordinate", and simple approximate procedures for constructing the transformations

$$r^* = r^*(r,\xi) \text{ and } \xi^* = \xi^*(r,\xi) \qquad (2)$$

have been described.[18,19] These are actually vector transformations and of course depend on the shape of the potential surface. In terms of r^*, ξ^*, and α^* the averaging procedure indicated in Eqs. (1) can be extended well into the canyon which leads to the product valley, and should remain a good approximation as long as the motion in ξ^* is much more rapid than that in r^*.

A precise formulation of the separability condition and related questions will not be attempted here. Many aspects of such a treatment would resemble closely the theory of vibration-rotation interactions.[15]

It should be noted that the average frequency of motion in the ξ^* coordinate actually may not drop very much even when the system "turns the corner" and enters the flared-out portion of the entrance valley. In Fig. 2, the zero-point energy and vibrational frequency associated with the ξ^* coordinate does drop by about a factor of 5 on going from an isolated HBr molecule to the middle of the turn; that is, from E_o = 3.8 kcal/mole, ω = 2650 cm^{-1} [see Fig. 1(b)]

to $E_o \approx 0.7$ kcal/mole, $\omega \approx 500$ cm^{-1} at $r \approx 3.2$ Å. However, it is possible that much of the original zero-point energy remains in the ξ^* motion as vibrational excitation. In this case the weighting factor in Eq. (1b) should be replaced by a sum of terms which account for the contributions from the various vibrational states.

Approximations for Rotational Coordinates

The proper treatment of the angle dependence of the potential and the various rotational terms in the kinetic energy is complicated, and in general the averaging will vary with the collision energy and angular momentum. There is little information about the angular dependence of intermolecular forces.[20] In Figs. 2 and 3 we have assumed a collinear configuration of the atoms, although it is likely that for reactions involving atoms with p orbitals a bent configuration would be more stable.[21] Also, a considerable fraction of the nonreactive collisions may be rotationally inelastic.[22,23,24]

There are some redeeming features. In most nonreactive collisions the orbital angular momentum L associated with the relative motion of A and BC about the center of mass is much larger than the rotational momentum J of the BC molecule. The kinetic terms involving BC rotations then can only slightly displace the trajectories from the plane perpendicular to $\underset{\sim}{L}$; thus the trajectories will at least qualitatively resemble those for a central force potential. This should hold also for the rotationally inelastic collisions if, as seems likely, the dominant transitions have $\Delta J \ll L$ and the energy transferred is small compared with the translational energy.

The potential energy function probably is strongly directional, but this also need not preclude the use of two-body central force mechanics. The angle of deflection in a collision is mainly determined by the interaction in the vicinity of the distance of closest approach, and ordinarily this region is traversed too quickly to permit much change in the relative orientation of A and

BC. Thus it is a plausible approximation to assume that in a given collision only one relative orientation is effective and to evaluate the deflection as if the angle α were fixed throughout the collision.[25] The deflections calculated for collisions with different fixed orientations should then be suitably averaged. For turning points at sufficiently large r (corresponding to small angle scattering), the various orientations may have almost equal weight, since here the dependence of the potential energy on α is weak compared with the average rotational energy of BC. The effect of the noncentral part of the potential may practically vanish in the uniform average over all orientations. On the other hand, for turning points in the region corresponding to the onset of chemical interaction, only a small range of orientations may be significant, if the dependence on α becomes strong enough to draw the BC molecule into the most favorable orientation before it has reached the turning point. In this case, the scattering would again appear to come from a central potential.

It is hoped that eventually these speculations may be tested by comparison with exact trajectory calculations for a three-body potential. With modern computers such calculations are feasible, and some studies of reactive scattering have already been made.[26] At present, however, a rigorous computer analysis of elastic scattering appears to be prohibitively expensive. A computer study of the elastic scattering of atoms from a rigid rotor molecule is in progress.[27]

The scattering patterns which we shall calculate from two-body mechanics would always be more or less blurred out if proper account were taken of rotational coordinates and inelastic and reactive scattering. For example, in the three body problem only the total angular momentum $\underset{\sim}{L} + \underset{\sim}{J}$ is a constant of the motion, and this suggests that the blurring effect of the kinetic rotational terms can be roughly estimated by averaging the two-body deflection function over a range $L + \bar{J}$ to $|L - \bar{J}|$ about the nominal value of L. Classically, the orbital angular momentum (in units of $\hbar$) is given by

4.558

$$L = 4.558\ (\mu E)^{\frac{1}{2}} b, \qquad (3)$$

in terms of the reduced mass μ (in gm/mole), relative kinetic energy E (in kcal/mole) and impact parameter b (in Angstrom units). The range $|\underset{\sim}{L} + \underset{\sim}{J}|$ to $|\underset{\sim}{L} - \underset{\sim}{J}|$ is only about 3% in a collision of K + HBr with relative energy E = 1 kcal/mole and impact parameter b = 6.3 Å (which corresponds to the "rainbow" minimum at K = 2, β = 1.3 in Fig. 7) and becomes 10% at b = 2 Å (or β = 0.4). Since the total reaction cross section is $Q_r \approx 5$ Å^2, attenuation by reaction is not expected to become dominant until $b \gtrsim (Q_r/\pi)^{\frac{1}{2}} \approx 1.5$ Å (or $\beta \gtrsim 0.3$). The K + CH_3Br and K + Br_2 systems are expected to be less favorable cases, since for rainbow collisions under similar conditions the range $|\underset{\sim}{L} + \underset{\sim}{J}|$ to $|\underset{\sim}{L} - \underset{\sim}{J}|$ becomes 12% and 35%, respectively. In fact, the rainbow pattern is found[1,2] to be quite sharp for K + HBr, it is considerably smeared out for K + CH_3Br and it is not observed at all for K + Br_2.

POTENTIAL FUNCTION

The central force potential chosen for this study is shown in Fig. 4, together with several of the effective potential curves,

$$U(r,L) = V(r) + \frac{L^2}{2\mu r^2}, \qquad (4)$$

obtained by adding the "centrifugal repulsion" term. The usual Lennard-Jones potential is used outside the van der Waals minimum at $r = r_m$, $V(r_m) = \varepsilon$. Within r_m the potential falls monotonically and below 0.7 r_m joins an inner, "chemical" well. This also has the Lennard-Jones form, with a minimum at $r'_m = 0.56\ r_m$ and $\varepsilon' = 5\varepsilon$. The ratio r'_m/r_m corresponds to the ratio of the bond length of KBr (2.82 Å) and the radius of the van der Waals well for K + HBr (5.1 Å). The ratio ε'/ε was taken as 5 to facilitate the use of available tables of deflection angles. This is somewhat less than the ratio of the exothermicity of the K + HBr reaction (3.8 kcal/mole) to the van der Waals well depth (0.52 kcal/mole).

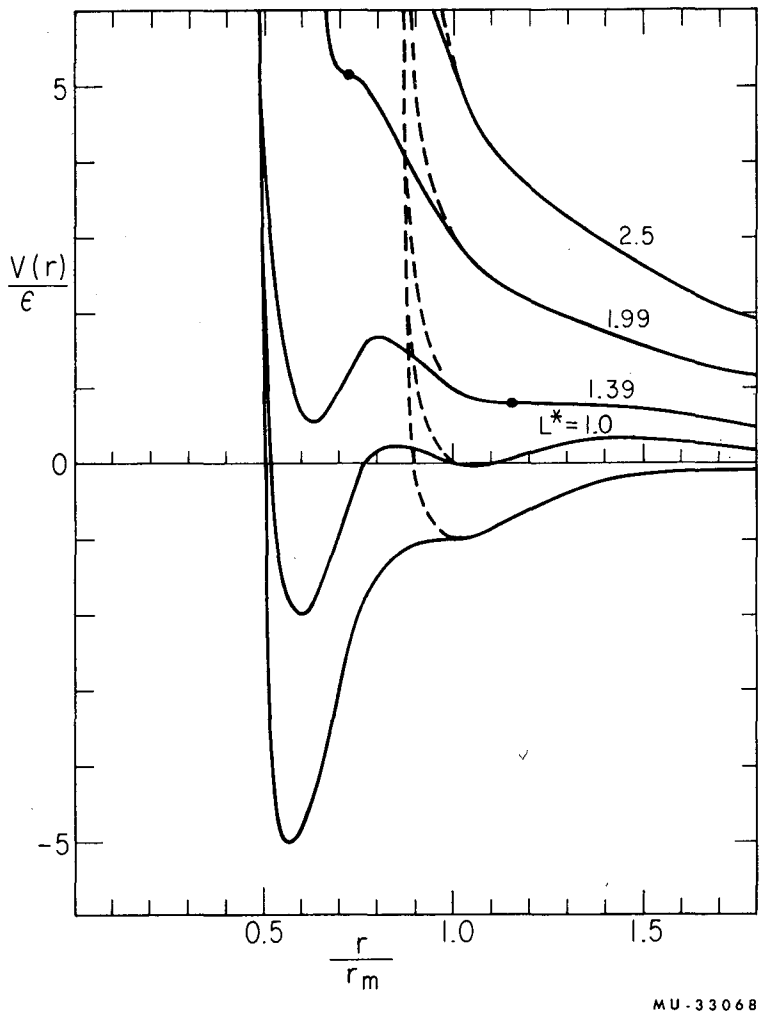

Fig. 4

The effective potential curves correspond to various values of a reduced angular momentum parameter,

$$L^* = L/\hbar B^{\frac{1}{2}} = K^{\frac{1}{2}}\beta. \tag{5}$$

Here $B = 2\mu\epsilon r_m^2/\hbar^2$ is the "capacity" parameter for the outer well, $K = E/\epsilon$ is the reduced kinetic energy, and $\beta = b/r_m$ the reduced impact parameter. For $r > r_m$, the $U(r,L^*)$ curves coincide with those for the usual Lennard-Jones potential, of course, and in particular for any $L^* < 1.39$ the outer region presents a centrifugal barrier. For $r < r_m$, the chemical well pulls the curves strongly downwards, and when $L^* < 1.99$ there appears an inner centrifugal barrier. The heavy dots in Fig. 4 (and Fig. 9) indicate the "triple points" for the outer and inner wells, located at

$$U = 0.8\epsilon,\ \beta = 1.75,\ L^* = 1.39 \tag{6}$$

and

$$U = 5.16\epsilon,\ \beta = 0.87,\ L^* = 1.99, \tag{7}$$

respectively. For K or L^* above these critical values, the corresponding portion of the effective potential curve is monotonic. At

$$U = 0.35,\ \beta = 1.76,\ L^* = 1.04 \tag{8}$$

the inner and outer centrifugal barriers have the same height; above this point the inner barrier is the higher, below it the outer barrier is the higher.

SEMICLASSICAL ANALYSIS

The general features of a semiclassical description of scattering from the two-well potential are illustrated in Figs. 5 - 9. Our analysis is based on the treatment outlined by Ford and Wheeler,[28] in which the classical deflection function plays the principal role. The deflection angle is given by

$$\Theta(K,\beta) = \pi - 2b \int_{r_c}^{\infty} \left[1 - \frac{b^2}{r^2} - \frac{V(r)}{E}\right]^{-1/2} r^{-2} dr, \qquad (9)$$

and depends only on the potential outside the distance of closest approach, $r = r_c$ (see Figs. 5 and 6), which is given by

$$r_c = b\left[1 - \frac{V(r_m)}{E}\right]^{-1/2}. \qquad (10)$$

Thus, for impact parameters such that $r_m \leq r_c$, the deflection is identical to that for the Lennard-Jones potential and can be obtained from published tables.[6] Also for turning points near a steeply rising portion of the effective potential curve, the dominant contribution to the deflection comes from the vicinity of $r = r_c$, since the integrand of (9) becomes very large there and is small elsewhere. Therefore, when r_c is well below r_m, the deflection approaches that for a Lennard-Jones potential with the inner well parameters r'_m and ε'. The contribution of the outer well can be approximated by replacing E by $E + \varepsilon$, as illustrated in Eq. (7), where the upper triple point is found to be located near $E = 5\,(0.8\varepsilon) + \varepsilon = 5\varepsilon$. For $K > 2$ we simply integrated Eq. (9) numerically for one or two of the impact parameters which produce turning points within the intermediate range, $0.7\, r_m$ to r_m, and interpolated between the inner and outer portions of the curve which were obtained from the tables. For $K < 2$, the perturbation by the outer well grows stronger and this treatment of the $r_c < r_m$ region becomes unsatisfactory because the integrand in (6) exhibits another large maximum well outside the turning point region. However, for $K < 5.16$, the inner well produces orbiting and the form of the inner part of the deflection curve can be determined, without integration, from the location and shape of the centrifugal barrier and the critical impact parameter for orbiting.[5,28] Thus again it was only necessary to locate two or three intermediate points by numerical

integration. The reduced phase shift was derived from the semiclassical relation,[28]

$$\frac{1}{2}\Theta = \hbar(\partial\eta/\partial L)_E. \qquad (11)$$

Since $\eta \to 0$ as $L \to \infty$, this yields

$$B^{-1/2}\eta(K,\beta) = -\frac{1}{2}K^{1/2}\int_\beta^\infty \Theta(K,\beta)d\beta. \qquad (12)$$

The orbiting singularities in the deflection angle produce abrupt jumps in the phase shift, which were smoothed out by the use of an improved approximation similar to Ford and Wheeler's "enlightened primitive JWKB analysis".

The most striking features of the scattering curves in Fig. 7 are the orbiting singularities, where Θ becomes infinite, the "rainbows", has an extremum and η an inflection, and the "glory", where Θ passes through zero and η has a maximum. The glory resembles that for the Lennard-Jones potential but is shifted to smaller impact parameters and has a somewhat different energy dependence. For $K > 5.16$ there are three rainbows. The outer minimum is identical to the rainbow of the Lennard-Jones potential, and the inner minimum is similar but deeper, in accord with the greater strength of the chemical well. In the angular distribution, these produce the usual "negative" rainbow; that is, they focus the intensity from the corresponding range of impact parameters into angles smaller than the extremum angle. However, the intermediate maximum in the deflection function produces a "positive" or "inverted" rainbow, with its "dark side" toward small angles and its "bright side" toward large angles. For $K < 5.16$, the inner negative rainbow is superseded by an orbiting singularity, and for $K < 0.8$ the outer rainbow likewise gives way to orbiting. As K is decreased further, the inner and outer orbiting singularities move closer together, with the positive rainbow squeezed between them, until they merge for $K \lesssim 0.35$.

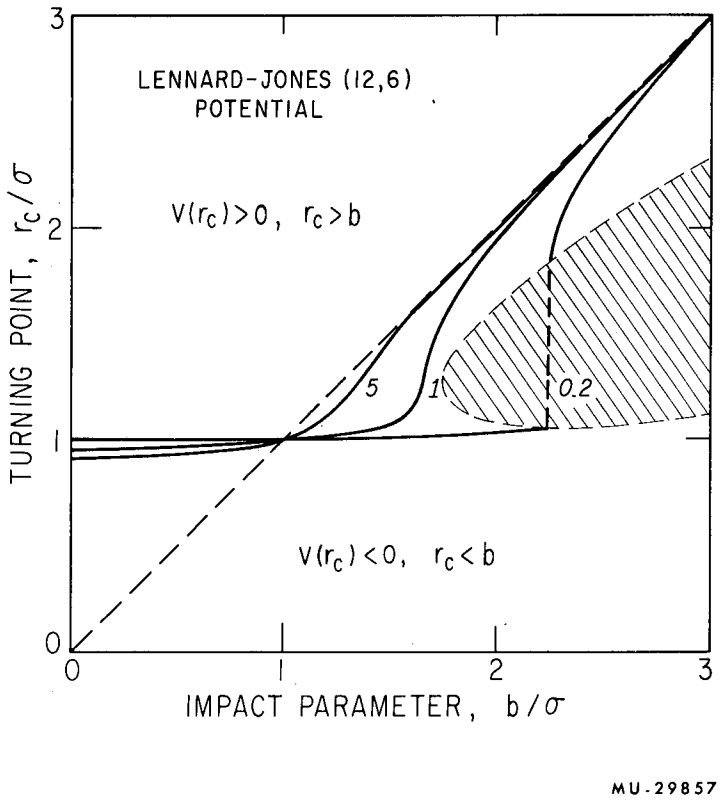
LENNARD-JONES (12,6)
POTENTIAL
V(r_c)>0, r_c>b
V(r_c)<0, r_c<b
5
1
0.2
TURNING POINT, r_c/σ
IMPACT PARAMETER, b/σ
0
1
2
3
MU-29857

Fig. 5

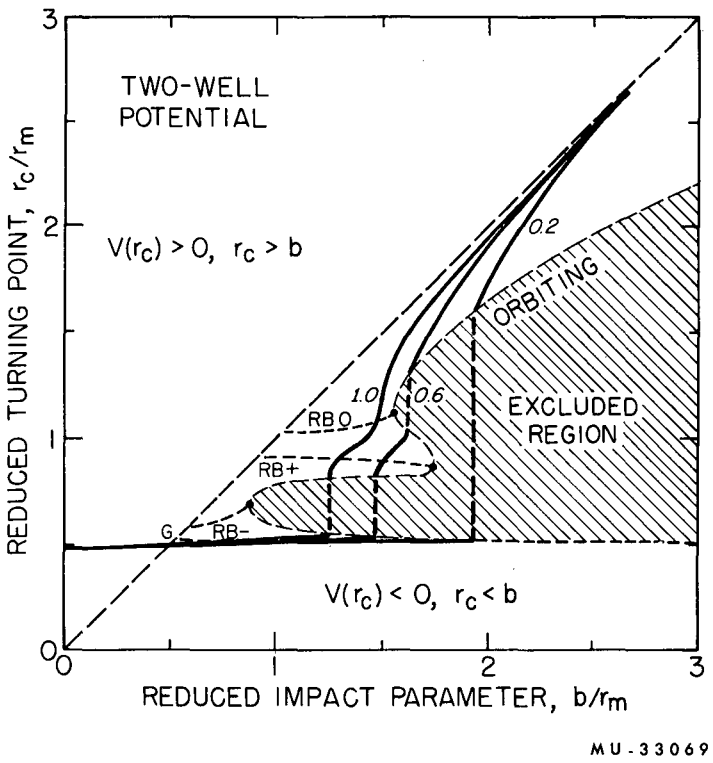
TWO-WELL
POTENTIAL
$V(r_c) > 0,\ r_c > b$
$V(r_c) < 0,\ r_c < b$
ORBITING
EXCLUDED
REGION
0.2
0.6
1.0
RB0
RB+
RB-
G
REDUCED TURNING POINT, r_c/r_m
REDUCED IMPACT PARAMETER, b/r_m
0
1
2
3
MU-33069

Fig. 6

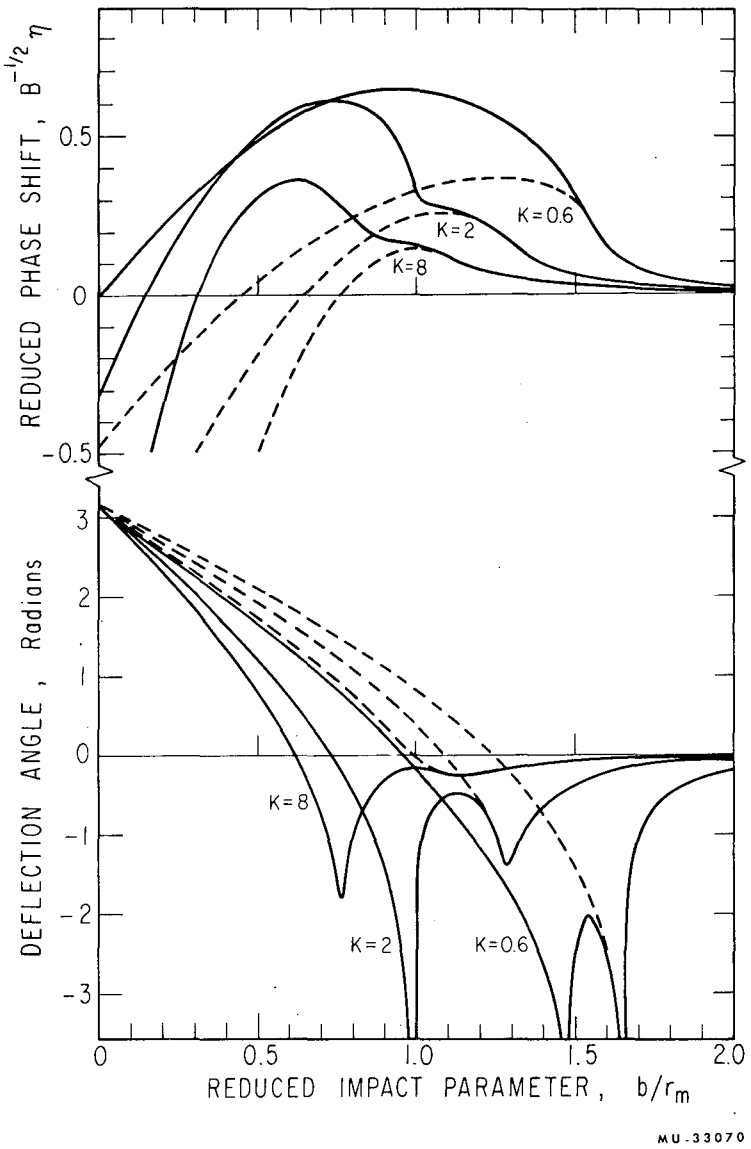
REDUCED PHASE SHIFT, $B^{-1/2}\eta$
0.5
0
-0.5
K=0.6
K=2
K=8
DEFLECTION ANGLE, Radians
3
2
1
0
-1
-2
-3
K=8
K=2
K=0.6
0
0.5
1.0
1.5
2.0
REDUCED IMPACT PARAMETER, b/r_m
MU-33070

Fig. 7

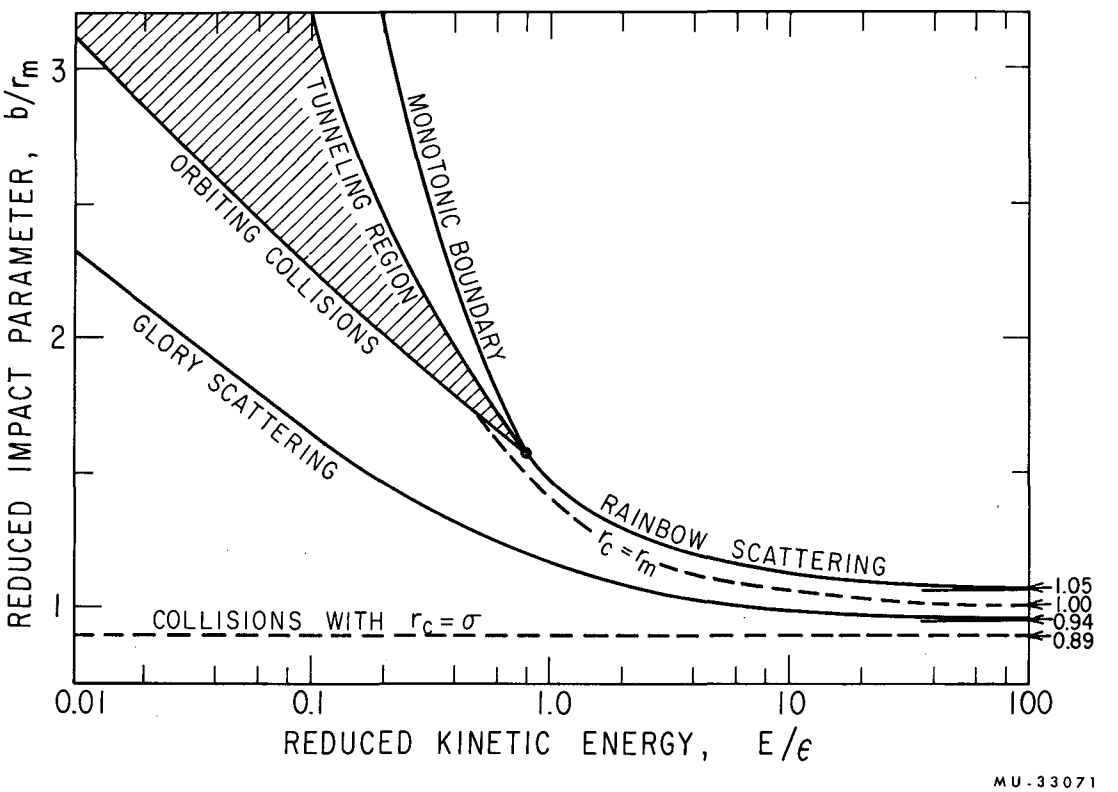
REDUCED IMPACT PARAMETER, b/r_m
3
2
1
TUNNELING REGION
ORBITING COLLISIONS
MONOTONIC BOUNDARY
GLORY SCATTERING
RAINBOW SCATTERING
$r_c = r_m$
COLLISIONS WITH $r_c = \sigma$
1.05
1.00
0.94
0.89
0.01
0.1
1.0
10
100
REDUCED KINETIC ENERGY, E/ϵ
MU-33071

Fig. 8

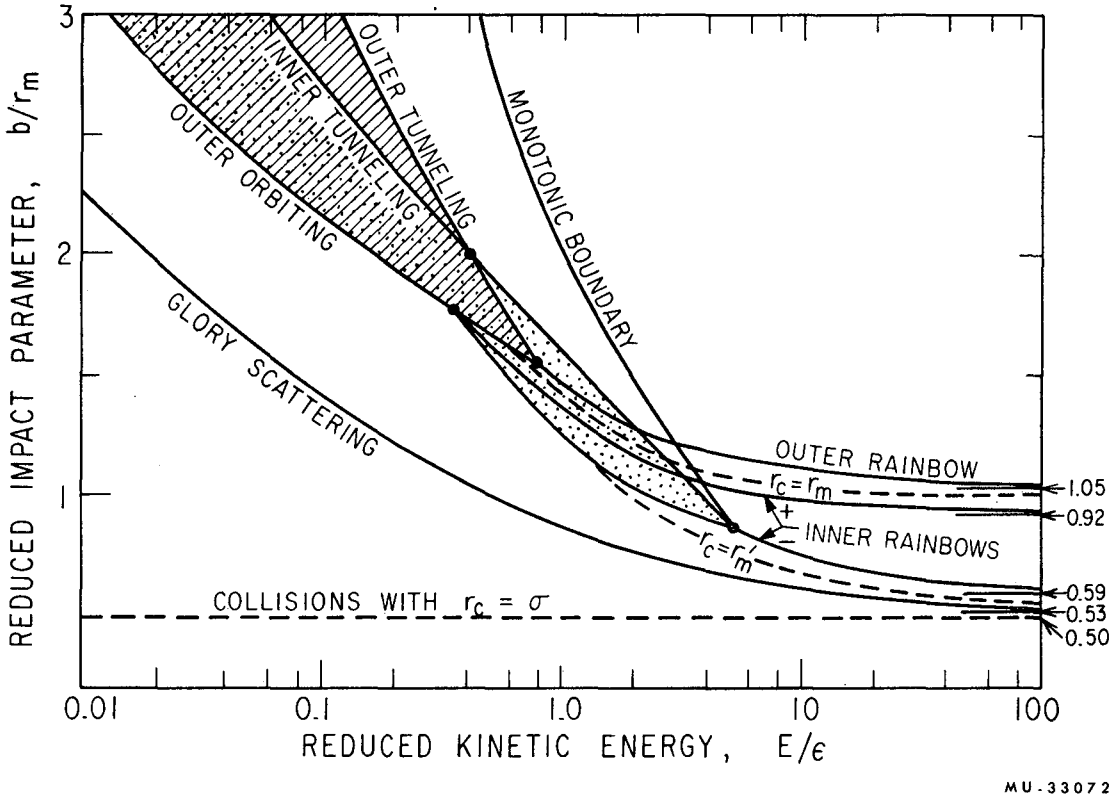
REDUCED IMPACT PARAMETER, b/r_m
REDUCED KINETIC ENERGY, E/ε
3
2
1
0.01
0.1
1.0
10
100
OUTER TUNNELING
INNER TUNNELING
OUTER ORBITING
MONOTONIC BOUNDARY
GLORY SCATTERING
OUTER RAINBOW
r_c = r_m
INNER RAINBOWS
r_c = r'_m
COLLISIONS WITH r_c = σ
1.05
0.92
0.59
0.53
0.50
MU-33072

Fig. 9

The topology of the scattering as a function of relative kinetic energy and impact parameter is shown in Fig. 8 for the Lennard-Jones potential and in Fig. 9 for the two-well potential. Below the glory scattering curve, repulsion predominates and the deflection is positive, above it attraction predominates and the deflection is negative. To the right of the "monotonic boundary", centrifugal repulsion outweighs the attractive interaction and the effective potential curve increases smoothly as r decreases. Within the doubly shaded area there exist two distinct, classically inaccessible regions, which can be reached by tunnelling through one or both of the centrifugal barriers; within the singly shaded areas there exists only one such region. Below the orbiting curves, the kinetic energy in the collision exceeds the centrifugal barriers. The dashed curves in Figs. 8 and 9 specify the conditions which produce turning points at the indicated radii. It is seen that the loci of the negative rainbows occur at roughly constant distances of closest approach, about 6% larger than those corresponding to the minima of the potential wells. Similarly, the glory occurs at a radius somewhat outside the repulsive core, where $V(\sigma) = 0$.

ANGULAR DISTRIBUTION

It is convenient to use the reduced polar cross section defined by

$$F(\theta) = 2\pi \sin\theta \; I(\theta)/\pi r_m^2, \tag{13}$$

where $I(\theta) = d(\pi b^2)/d\omega$ is the customary differential cross section per unit solid angle in the center-of-mass system. In the classical approximation,

$$F(\theta) = 2\beta(\theta)/|\partial\Theta/\partial\beta|, \tag{14}$$

and depends only on the reduced energy K once the form of the potential is specified. The semiclassical approximation[28] introduces quantum correction factors which depend on the capacity parameter B as well as K, but ordinarily

these are only significant for the rainbow scattering and sometimes for glory scattering. It is convenient to analyze separately various contributions to the angular distribution which arise from particular portions of the classical deflection function. Table II gives such an analysis for four branches of the deflection function which can be approximated by simple functions. The complete angular distribution is readily synthesized from these formulas plus the contribution from the "repulsive branch" of the deflection function (the region with $\beta < \beta_g$ in Fig. 7), which is evaluated numerically from Eq. (14). A summary of notation, units, and convenient working formulas is given in Table III.

The contributions from rainbow, orbiting, and glory scattering all consist of a characteristic "form factor" which involves dimensionless "width" and "height" parameters. The derivation of these formulas merely amounts to rearranging the results of Ford and Wheeler.[28] The form factors for rainbow and glory scattering are given in Table IV and Fig. 10; the factor for orbiting is just a simple exponential function. Reduced forms of the various width and height parameters that depend only on the reduced kinetic energy are plotted in Figs. 11 - 13 over the range K = 0.1 to 100.

As indicated in Table II, these parameters depend on the form of the potential function via the following properties of the classical deflection function:

For rainbow scattering,

$$\beta_r,\ \theta_r,\ \text{and}\ a_r = \frac{1}{2}(\partial^2\Theta/\partial\beta^2)_r$$

For orbiting,

$$\beta_o,\ \theta_o,\ \text{and}\ a_o$$

For glory scattering,

$$\beta_g\ \text{and}\ a_g = (\partial\Theta/\partial\beta)_g.$$

These quantities were evaluated by numerical analysis. For the two-well potential, the approximate deflection functions illustrated in Fig. 7 were used, and for the Lennard-Jones potential the extensive tabulation of Hirschfelder, Curtiss, and Bird.[6] Simple analytic expressions can be obtained in the high energy region, where Eq. (12) reduces to the Born approximation result,

$$\eta = -\frac{1}{\hbar v}\int_b^\infty V(r)\left[1 - \frac{b^2}{r^2}\right]^{-1/2} dr. \tag{15}$$

For a potential of the form $V(r) = C/r^s$, this yields

$$\eta = -\frac{C}{\hbar v}\,\frac{F(s)}{b^{s-1}} \tag{16}$$

where

$$F(s) = \frac{(s-3)(s-5)\ldots 1}{(s-2)(s-4)\ldots 2}\,\frac{\pi}{2}, \text{ for } s \text{ even} \tag{17a}$$

$$= \frac{(s-3)(s-5)\ldots 2}{(s-2)(s-4)\ldots 3}, \text{ for } s \text{ odd} \tag{17b}$$

At the high energy limit, the deflection angle $\Theta = 2d\eta/d\ell$ and its derivatives are thus given by

$$\Theta = \frac{C}{E}\,\frac{(s-1)F(s)}{b^s} \tag{18a}$$

$$\frac{\partial\Theta}{\partial b} = -\frac{C}{E}\,\frac{s(s-1)F(s)}{b^{s+1}} \tag{18b}$$

$$\frac{\partial^2\Theta}{\partial b^2} = \frac{C}{E}\,\frac{s(s^2-1)F(s)}{b^{s+2}}, \tag{18c}$$

where the identity $\hbar v = 2\chi E$ has been used. Table V gives the limiting formulas obtained by applying these approximations to the Lennard-Jones potential,

Table II. Semiclassical analysis of angular distribution

Deflection Function	Reduced Polar Cross Section	Parameters
Attractive branch:		
$\Theta = -(15\pi/8)K\beta^6$	$0.759K^{-1/3}\theta^{-4/3}$	
Rainbow branch:		
$\Theta = \theta_r + a_r(\beta - \beta_r)^2$	$H_r(B,K)Ai^2(x)$	$x = (\theta - \theta_r)/\Delta\theta_r$ $\Delta\theta_r = B^{-1/3}K^{-1/3}a_r^{1/3}$ $H_r = 3.60B^{1/6}K^{5/6}\beta_r a_r^{2/3}$
Orbiting branch:		
$\Theta = \theta_o + a_o \ln\lvert(\beta - \beta_o)/\beta_o\rvert$	$H_o(K)\exp(-\theta/\Delta\theta_o)$	$\Delta\theta_o = a_o$ $H_o = (2\beta_o^2/a_o)\exp(-\theta_o/a_o)$
Glory branch:		
$\Theta = \theta_g + a_g(\beta - \beta_g)$	$H_g(K)G(y)$	$y = \lvert\sin\theta/\Delta\theta_g\rvert$ $G(y) = \pi y J_o^2(y)$ $\Delta\theta_g = B^{-1/2}K^{-1/2}\beta_g^{-1}$ $H_g = 4\beta_g/a_g$

Table III. Notation, units, and handy numerical formulas

E = relative kinetic energy = $\frac{1}{2}\mu v^2$, kcal/mole

L = orbital angular momentum = $\mu vb = (\ell + \frac{1}{2})\hbar$

v = relative velocity, 10^4 cm/sec

b = impact parameter = $(\ell + \frac{1}{2})\lambda$, Å

μ = reduced mass = $m_1 m_2/(m_1 + m_2)$, gm/mole

ϵ = potential well depth, kcal/mole

r_m = radius of potential minimum, Å

$\alpha = 1.2897\ (T/M)^{1/2}$, most probable velocity in oven

$v = 28.95\ (E/\mu)^{1/2}$

$E = 1.195 \times 10^{-3}\ \mu v^2$

$\lambda = 6.3522/\mu v = 0.2196\ (\mu E)^{-1/2}$

$\ell + \frac{1}{2} = 0.15743\ \mu vb = 4.558\ (\mu E)^{1/2} b$

$r_m = 2^{1/6}\sigma = 1.1225\sigma$ for Lennard-Jones potential

θ (radians) = 57.2958 θ (degrees), scattering angle

$A = r_m/\lambda = (BK)^{1/2} = DK$

$B = 2\mu\epsilon r_m^2/\hbar^2 = AD = D^2K$

$D = 2\epsilon r_m/\hbar v = B/A = A/K = (B/K)^{1/2}$

$K = E/\epsilon = A/D = A^2/B = B/D^2$

$\beta = b/r_m = (\ell + \frac{1}{2})/A$

$L^* = L/\hbar B^{1/2} = K^{1/2}\beta$

$A = 0.15743\ \mu v r_m = 4.558\ (\mu E)^{1/2} r_m$

$B = 21.3\ \mu\epsilon r_m^2$

$D = 135.5\ \epsilon r_m/v$

Table IV. Form factors for the rainbow and glory contributions.

x	$Ai^2(x)$ [a]	y	G(Y) [b]
0.50	0.195	0.0	0.000
0.00	0.438	0.1	0.308
-1.02	1.000	0.2	0.630
-1.75	0.438	0.3	0.918
-2.34	0.000	0.4	1.155
-3.25	0.612	0.5	1.493
-4.09	0.000	0.6	1.565
-4.82	0.505	0.7	1.710
-5.52	0.000	0.8	1.806
-6.16	0.446	0.9	1.848
-6.79	0.000	0.92	1.855
		1.0	1.835
		1.1	1.783
		1.2	1.700
		1.3	1.582
		1.4	1.350
		1.6	1.130
		1.8	1.050
		2.0	1.000

[a] Square of the Airy integral, normalized to unity at its maximum.

[b] Square of the zero order Bessel function multiplied by πy and smoothly joined to unity in the region $1.5 < y < 2$.

Table V. Small angle scattering approximation for the Lennard-Jones (6,12) potential.

$$V(r) = \epsilon\left[\left(\frac{r_m}{r}\right)^{12} - 2\left(\frac{r_m}{r}\right)^{6}\right]$$

$$\eta = \frac{3\pi}{16}\frac{D}{\beta^5}\left\{1 - \frac{21}{64}\frac{1}{\beta^6}\right\}$$

$$\Theta = -\frac{15\pi}{8}\frac{1}{K\beta^6}\left\{1 - \frac{231}{320}\frac{1}{\beta^6}\right\}$$

$$\partial\Theta/\partial\beta = \frac{45\pi}{4}\frac{1}{K\beta^7}\left\{1 - \frac{231}{160}\frac{1}{\beta^6}\right\}$$

$$\partial^2\Theta/\partial\beta^2 = \frac{-315\pi}{4}\frac{1}{K\beta^8}\left\{1 - \frac{429}{160}\frac{1}{\beta^6}\right\}$$

$\beta_g = 0.947$ $\qquad$ $\beta_r = 1.056$

$\eta_g = 0.422D$ $\qquad$ $\eta_r = 0.306D$

$a_g = -52.0/K$ $\qquad$ $\theta_r = -2.04/K$

$a_r = 63.5/K$

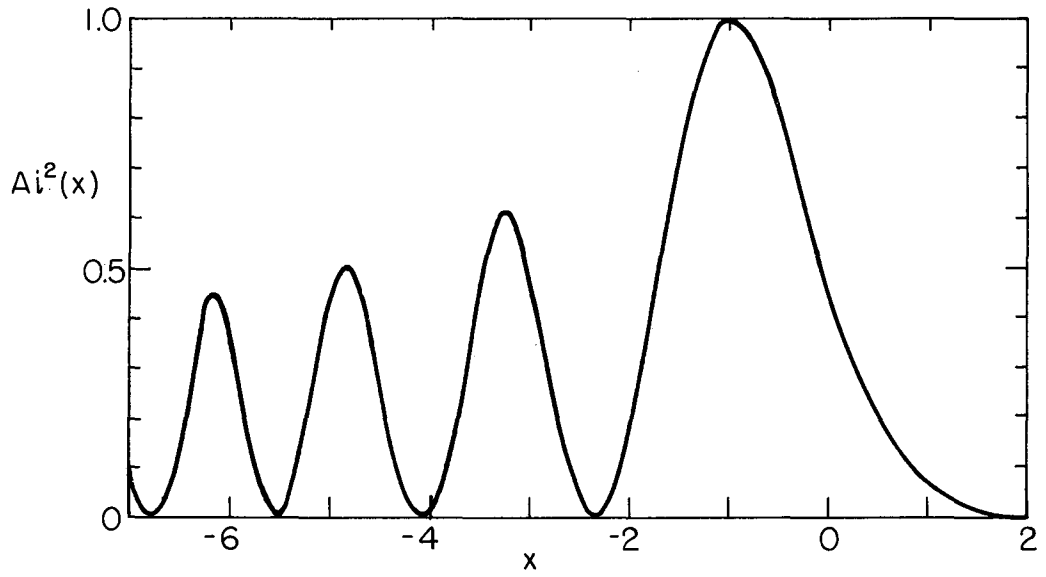

MU-33073

Fig. 10a

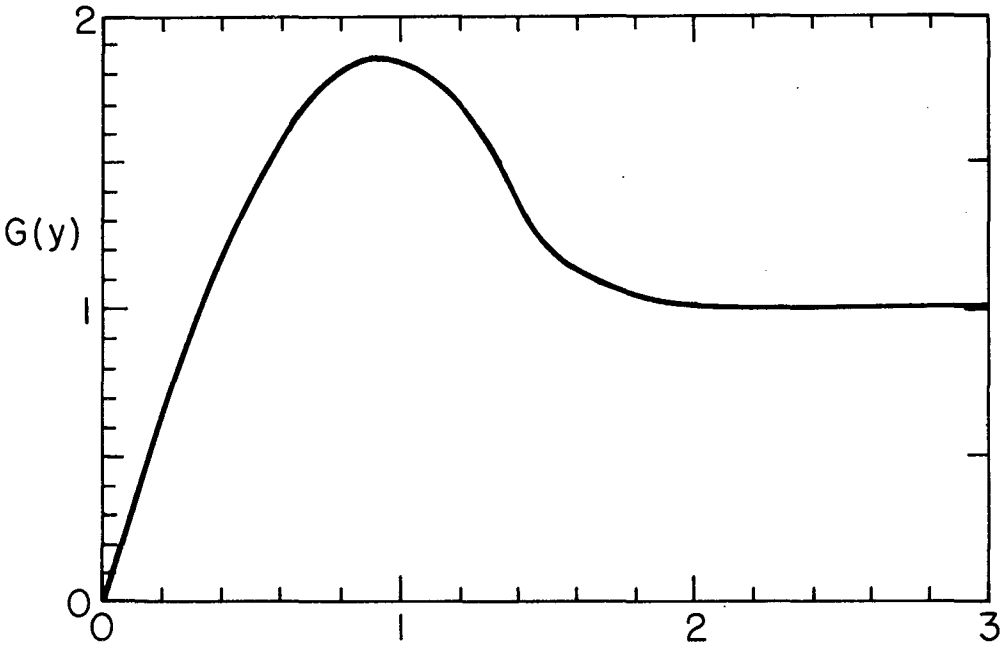

MU-33074

Fig. 10b

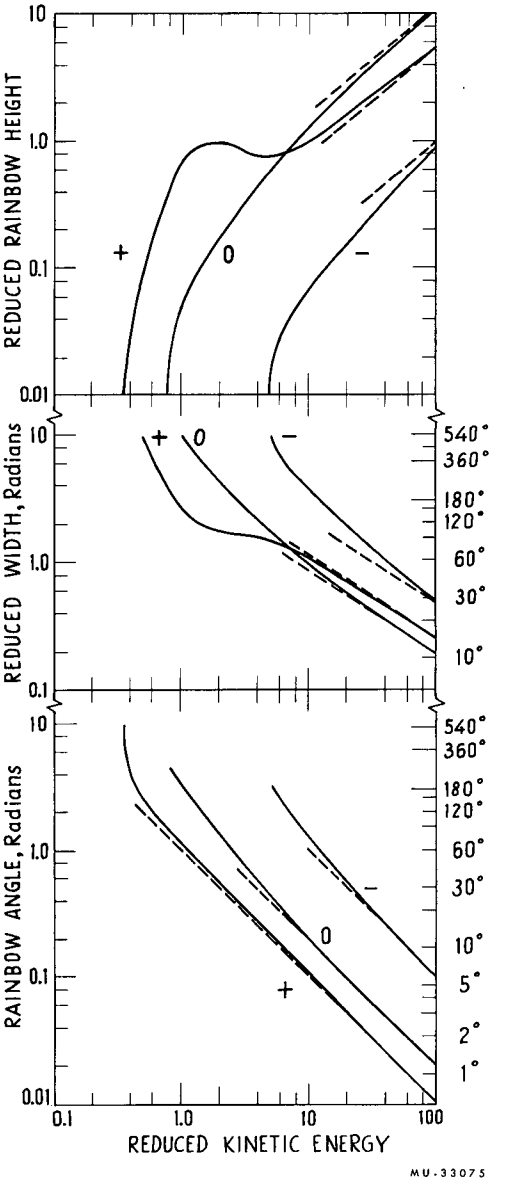
REDUCED RAINBOW HEIGHT
REDUCED WIDTH, Radians
RAINBOW ANGLE, Radians
REDUCED KINETIC ENERGY
10
1.0
0.1
0.01
0.1
1.0
10
100
+
0
−
540°
360°
180°
120°
60°
30°
10°
5°
2°
1°
MU-33075

Fig. 11

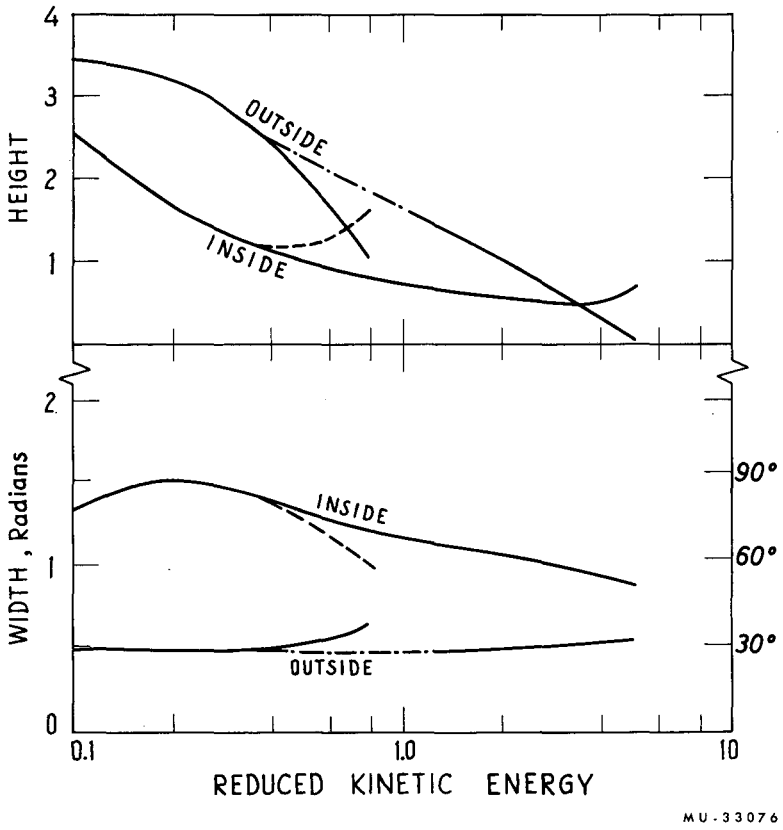
HEIGHT
4
3
2
1
OUTSIDE
INSIDE
WIDTH, Radians
2
1
0
INSIDE
OUTSIDE
90°
60°
30°
0.1
1.0
10
REDUCED KINETIC ENERGY
MU-33076

Fig. 12

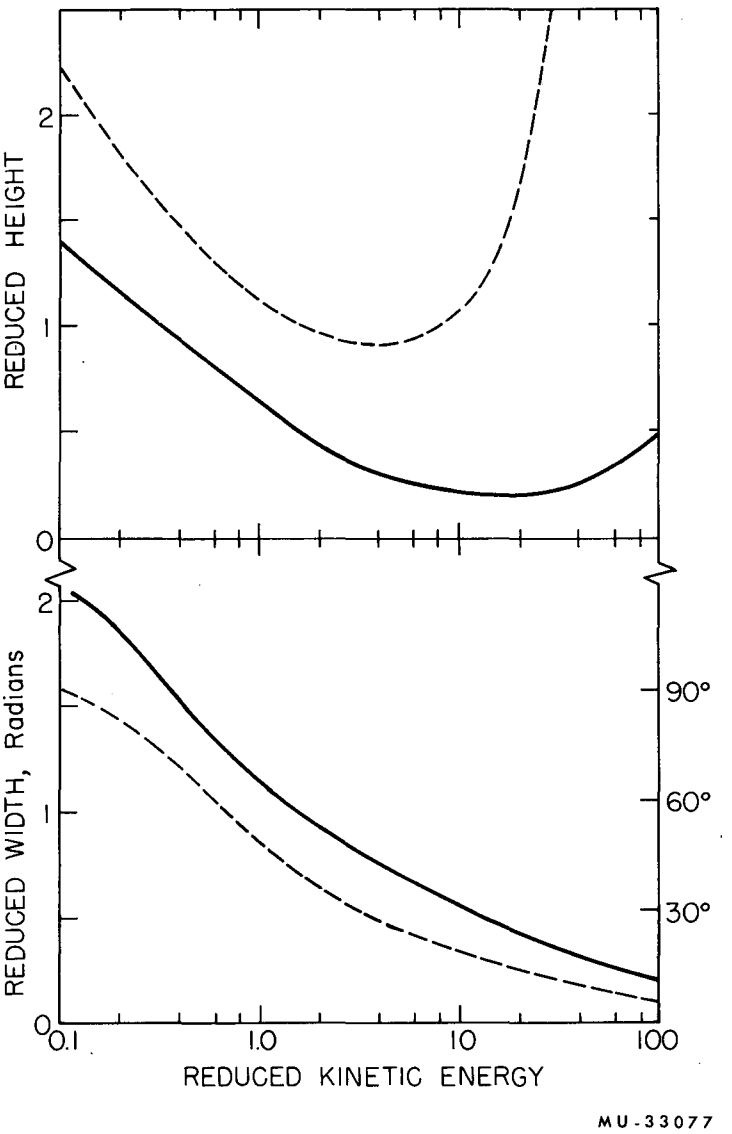
REDUCED HEIGHT
2
1
0
REDUCED WIDTH, Radians
2
1
0
90°
60°
30°
0.1
1.0
10
100
REDUCED KINETIC ENERGY
MU-33077

Fig. 13

together with the parameters for rainbow and glory scattering obtained from the conditions $(\partial\Theta/\partial\beta)_r = 0$ and $\Theta_g = 0$. For the two-well potential, similar formulas can be obtained by suitable adjustment of the scale factors, but the limiting forms will not hold until correspondingly higher energies are reached.

Fig. 14 shows the angular distributions which correspond to the deflection functions of Fig. 7. The rainbow contributions are evaluated for B = 5000, a value roughly appropriate to both the K + HBr and the K + CH_3Br cases. For smaller values of B, the rainbow bumps would be weaker and broader. (The glory effect form factor is unity except at very small angles and hence will be ignored.)

The fall-off in intensity at wide angles (for the moment, ignore the rainbow bumps) is seen to be considerably more rapid than that for the Lennard-Jones potential. At K = 8, the wide angle scattering comes entirely from the repulsive branch of the deflection function. For K < 5.16 there is also a contribution from inner orbiting; this falls off more rapidly but is roughly comparable in total intensity. For K < 0.8 there is a further contribution from outer orbiting. The fall-off in the total wide angle scattering is not quite as rapid and its onset is less abrupt than observed in the scattering of K + HBr and K + CH_3Br. The calculated distributions are found to change in this fashion when the repulsive wall is moved back further and the inner potential well is made deeper or broader. Thus it is not necessary to assume that the depletion by reaction is unexpectedly large, as these calculations indicate that the observed fall-off in wide angle scattering can be accounted for by a two-well potential with reasonable dimensions.

In principle the complicated rainbow structure can offer a sensitive test of the form of the potential. At K = 8, the inner positive rainbow (RB+) and the outer rainbow (RBO) patterns have comparable intensity and overlap near 12°. The

inner negative rainbow (RB-) gives rise to a principal maximum at 83° and a secondary maximum at 42°. The latter appears because the minimum in the deflection curve (see Fig. 7) is deep and sufficiently symmetrical to maintain the Airy interference pattern[28] over a wide angular range. At K = 2, the RB+ also produces two lobes, the principal one at 38°, the secondary one at 52°. These are considerably more intense than the RBO lobe at 61°, since in this energy range the maximum in the deflection function (see Fig. 7) is quite broad as a consequence of the extended "pause" in V(r) just below $r = r_m$. The RB- has disappeared, as it has passed through 180° and gone over to orbiting at K = 5.16. At K = 0.6, the RBO has also vanished and the RB+ pattern is smearing out as it moves to wide angles.

No evidence of the RB+ or RB- rainbow features has been found for the examples studied thus far.[1,2] The absence of an RB- pattern in the thermal energy range is not surprising, as the chemical well probably should be relatively deeper and broader than assumed here, and the triple point (7) moves rapidly to higher energy as the volume of the well is increased. Thus, in the thermal range the inner well should produce "chemical orbiting" rather than an RB- pattern. Enlarging the inner well also squeezes the RB+ pattern closer to the RBO pattern, since the inner dip in the deflection function (see Fig. 7) then sets in at larger impact parameters. This extends considerably the range of reduced energy over which the RB+ and RBO patterns cannot be separately resolved and likewise delays the appearance of "anomalous" intensity in the RB+ rainbow. For the experiments so far reported, $K \gtrsim 3$, and the observation of only a single rainbow bump is compatible with a potential qualitatively similar to that of Fig. 4 but with the volume of the inner well increased by about 50%. A decisive test of the multiple rainbow features implied by this form of the potential can only be obtained by experiments at energies which are either somewhat below the convenient thermal range (K small enough to permit the anomalous

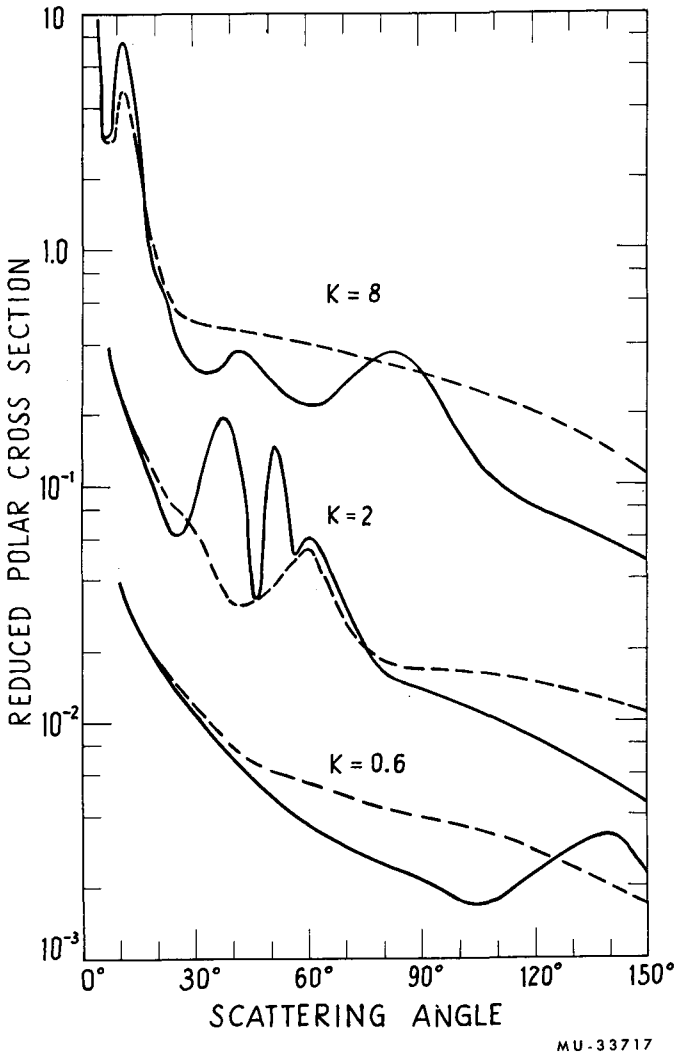
10
1.0
10^{-1}
10^{-2}
10^{-3}
REDUCED POLAR CROSS SECTION
K = 8
K = 2
K = 0.6
0°
30°
60°
90°
120°
150°
SCATTERING ANGLE
MU-33717

Fig. 14

RB+ pattern to emerge as the RBO broadens into orbiting) or well above it (K large enough to produce the RB- rainbow at wide angles).

TOTAL CROSS SECTION

The semiclassical treatment yields simple analytic formulas for the velocity dependence of the total elastic cross section. For thermal energy scattering from potentials qualitatively similar to the Lennard-Jones potential, the cross section may be resolved into two terms: $Q(v) = Q_o + \Delta Q_o$. The main term, Q_o, is a monotonically decreasing function of velocity and depends essentially only on the form of the interatomic potential at large distances.[29,30] The ΔQ term gives an undulatory fine structure and depends primarily on the size and shape of the attractive potential well. Bernstein has evaluated the functional dependence of ΔQ for a Lennard-Jones potential; however, his method required an extensive numerical analysis.[31]

General semiclassical approximations for both Q_o and ΔQ are readily obtained from the optical theorem.[32] The theorem gives

$$Q(r) = 4\pi\lambda \mathrm{Im} f(0), \tag{19}$$

where $f(0)$ is the forward scattering amplitude. In the semiclassical approximation,[28]

$$f(0) = (i/\lambda)\int_o^\infty (1 - e^{2i\eta})bdb. \tag{20}$$

The net contribution from the oscillatory $e^{2i\eta}$ factor is only appreciable when the phase shift remains almost constant over a significant range of impact parameters. For thermal scattering from simple one-well potentials, this occurs in two regions: (a) for "soft" collisions at large b, where only the weak attractive dispersion forces are significant and η becomes very small; and (b) for glory scattering near $b = b_g$, where the attractive and repulsive forces become comparable, the classical deflection angle passes through zero, and the phase shift passes through an extremum.

In region (a), the Born approximation of Eq. (16) may be used (with $s > 3$) and this gives

$$f(0) \simeq (\rho^2/2\lambda)\Gamma[(s-3)/(s-1)]e^{i\alpha} \tag{21a}$$

where

$$\rho = [(2|C|/\hbar v)F(s)]^{1/(s-1)} \tag{21b}$$

and the phase angle is

$$\alpha = \frac{\pi}{2} + \frac{\pi}{s-1}(C/|C|) \tag{21c}$$

Thus we obtain

$$Q_o = 2\pi\rho^2\Gamma[(s-3)/(s-1)] \cos[\pi/(s-1)]. \tag{22}$$

This result differs somewhat from the original Massey-Mohr approximation[29] but is identical to that obtained from the Schiff-Schlier and Landau-Lifshitz methods.[30]

In region (b), the deflection function is approximately linear (see Table II) with impact parameter,

$$\Theta = a_g(\beta - \beta_g), \tag{23a}$$

and since $\Theta = 2d\eta/d\ell = (2/A)d\eta/d\beta$, the phase shift is approximately quadratic,

$$\eta = \eta_g + \frac{1}{4}a_g A(\beta - \beta_g)^2. \tag{23b}$$

Thus, as shown by Ford and Wheeler,[28]

$$f_g(0) \simeq b_g(2\pi A/|a_g|)^{1/2} e^{i\alpha_g} \tag{24a}$$

where

$$\alpha_g = 2\eta_g + \frac{1}{4}\pi(a_g/|a_g|) - \frac{1}{2}\pi . \tag{24b}$$

Hence the undulatory contribution is

$$\Delta Q = 4\pi\lambda b_g(2\pi A/|a_g|)^{1/2}\cos 2\pi N \tag{25}$$

where

$$N = (\alpha_g + \frac{3}{2}\pi)/2\pi \tag{26}$$

is introduced as a convenient index for the extrema. N = 1, 2, 3,... for maxima and N = 3/2,5/2,... for minima. From the definition of α_g, the condition for an extrema is

$$|\eta_g| = \pi(N - \tfrac{3}{8}) \tag{27a}$$

if η_g and a_g are opposite in sign ("negative" glory scattering, the usual case), and

$$|\eta_g| = \pi(N - \tfrac{5}{8}) \tag{27b}$$

if η_g and a_g have the same sign ("positive" glory scattering).

In terms of the dimensionless parameters of Tables II and III, we have

$$Q_o/\pi r_m^2 = 2.54\ D^{2/5} = 2.54\ (B/K)^{1/5} \tag{28}$$

$$\Delta Q/\pi r_m^2 = 10.03\ A^{-1/2}\ \beta_g |a_g|^{-1/2} \cos 2\pi N \tag{29a}$$

$$= 10.03\ D^{-1/2}\ \beta_g |Ka_g|^{-1/2} \cos 2\pi N \tag{29b}$$

$$= 10.03\ B^{-1/4}\ \beta_g K^{-1/4} |a_g|^{-1/2} \cos 2\pi N \tag{29c}$$

$$= 5.015\ \beta_g (H_g \Delta\theta_g)^{1/2} \cos 2\pi N\ . \tag{29d}$$

We shall use the forms involving the velocity independent parameter B. The amplitude of the undulatory contribution is readily determined from the glory scattering parameters of Table II and Fig. 13. The glory phase shift, η_g, which governs the wavelength of the undulations, is evaluated from Eq. (12) and Table V. Fig. 15 gives the reduced phase shift, $B^{-1/2}\eta_g$, and the reduced relative amplitude, $B^{9/20}U$, where

$$\Delta Q/Q_o = U \cos 2\pi N \tag{30}$$

and

$$U = 3.95\ B^{-9/20} \beta_g K^{-1/20} |a_g|^{-1/2}. \tag{31}$$

For the Lennard-Jones potential, Eqs. (28) and (30) approximate the results of exact partial wave calculations within a few percent.[31] They become inapplicable in the "high velocity" region where η_g is very small and repulsive

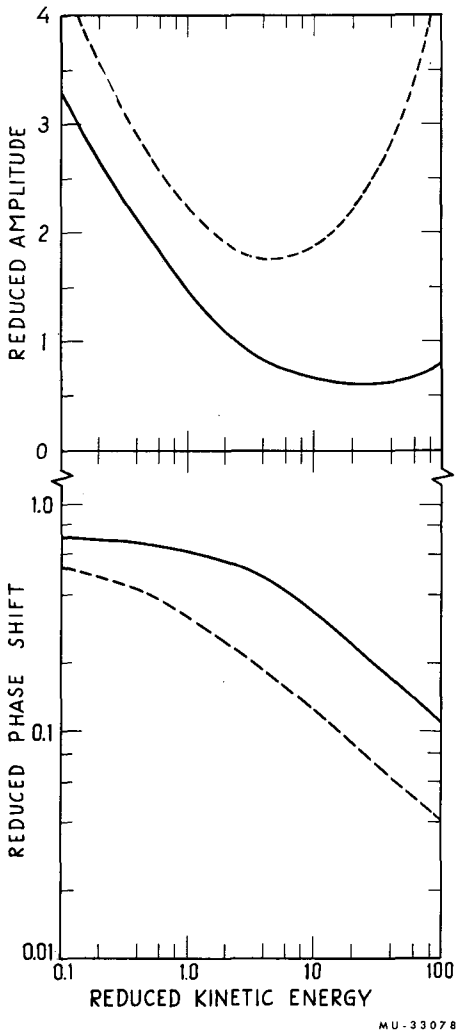
4
3
2
1
0
REDUCED AMPLITUDE
1.0
0.1
0.01
REDUCED PHASE SHIFT
0.1
1.0
10
100
REDUCED KINETIC ENERGY
MU-33078

Fig. 15

phase shifts dominate, and they are at best incomplete in the "orbiting" region where the usual semiclassical procedures are inadequate.[28] Thus their range of application is roughly

$$2 \lesssim D \lesssim B^{1/2}. \tag{32}$$

About half of the maximum number of undulations permitted by Levinson's theorem[31] will occur in the orbiting region.

Bernstein[31] has derived two semiclassical approximations for ΔQ; the first agrees with the undulation amplitude in Eq. (29) but has $\frac{1}{4}$ instead of $\frac{3}{8}$ in the extrema condition of Eq. (27a); the second gives amplitudes about 35% too large.

For the two-well potential the wavelength of the undulations (spacing between the velocities corresponding to extrema in ΔQ) is less than that for the Lennard-Jones potential in roughly the ratio $\varepsilon r_m/\varepsilon' r'_m \simeq 1/3$. The amplitude is also less by a factor of about $r'_m/r_m \simeq 1/2$. As the glory effect appears at rather small impact parameters, it may prove to be drastically weakened by rotational blurring. Otherwise, however, the measurement of $\Delta Q(v)$ should provide a direct test for the presence of the inner chemical well. Such measurements have not yet been reported for the scattering of reactive molecules, although $\Delta Q(v)$ has been determined for several atom-atom systems.[33]

OTHER TWO WELL POTENTIALS

If the repulsive wall in Fig. 4 is removed and the inner well given a broad, flat bottom, then for impact parameters inside the rainbow region the deflection angle approaches zero again and the phase shift becomes practically constant. This further suppresses the wide angle scattering but does not qualitatively change the rainbow structure of the angular distribution. Despite the absence of a glory, if the region of constant phase is sufficiently broad $Q(y)$ can show an undulatory velocity dependence that is markedly larger in amplitude than for a Lennard-Jones potential.

If the inner and outer wells are separated by a potential barrier, the scattering at energies below the barrier top is essentially the same as that from a Lennard-Jones potential. At higher energies, the inner well produces a strong downward dip in the deflection function and thus introduces a glory with positive slope ($a_2 > 0$) in addition to the usual glory (with $a_1 < 0$) present for Lennard-Jones scattering. Each of these gives an oscillatory contribution to the total cross section,

$$\Delta Q = U_1 \cos 2\pi N_1 + U_2 \cos 2\pi N_2. \qquad (33)$$

Thus the velocity dependence may show a "beat" pattern in which the wavelength increment essentially measures the difference in the area of the van der Waals well and the area of the activation energy barrier.

DISCUSSION

The main point illustrated by these calculations is that the fall-off in wide-angle elastic scattering which has been observed for several reactive systems[1-4] may arise primarily from the "softness" of the potential. Comparison with the experimental reaction cross sections indicates that depletion by reaction is a much less significant factor. Since we have had to use two-body central force mechanics in order to carry out any detailed analysis, the various special features we have predicted are quite dubious and may turn out to be unobservable. However, even if this occurs, it should be possible to obtain at least a qualitative experimental characterization of the potential inside the region which would be excluded by the repulsive core in collisions of nonreactive molecules. For this purpose, even experiments without velocity selection will be useful, especially for systems in which the chemical well is deep compared with thermal energies. In terms of experimental motivation, this is an important contrast with the interpretation based on depletion;[1-3] the latter requires velocity selection, to permit an impact parameter to be assigned to each scattering angle.

Perhaps we should emphasize that despite our frequent reference to the K + HBr system, the potential we have used is not likely to be appropriate for this system. The observed threshold for chemical reaction of 0.4 kcal/mole indicates the presence of a positive potential barrier.[1] Also, as mentioned already, in the region of the potential surface which is important for elastic scattering most of the initial zero point vibrational energy of HBr may remain associated with the ξ^* coordinate rather than entering the reaction coordinate. In this case, the effective potential for elastic scattering would not display a chemical well nearly as deep as that of Fig. 4. If there is an appreciable potential drop beyond the barrier, however, the K + HBr scattering should possess a chemical glory of strength comparable to the usual van der Waals glory. Hence this appears to be a promising system with which to look for a beat pattern in the velocity dependence of the total cross section.

FIGURE CAPTIONS

Fig. 1 - (a) Exp-6 ($\alpha = 12$) potential function for K + HBr. The potential vanishes at $r = \sigma$ and has its minimum, $-\epsilon$, at $r = r_m$.
(b) Harmonic oscillator vibrational potentials for HBr and KBr. Dotted lines indicate the zero-point vibrational levels.

Fig. 2 - Contour map of potential energy surface for linear configurations of the HBr + K system. Dashed contours indicate the potential surface (derived from Table I) which would obtain if there were no chemical interaction but only van der Waals interaction. Arrows show location of van der Waals minima at $r = r_m$ and equilibrium bond lengths at $r = r_e$.

Fig. 3 - Magnified view of the HBr + K entrance valley in the potential surface of Fig. 2. The translational coordinate is the K - Br distance, the vibrational coordinate is the H - Br distance. Trajectory shown at right corresponds to an initial relative velocity of HBr and K of 10^5 cm/sec, with HBr in the ground vibrational state. Arrows at left indicate the zero-point vibrational amplitude.

Fig. 4 - Two-well potential and effective potential energy curves for various values of the reduced angular momentum. The corresponding curves for the Lennard-Jones potential are shown dashed.

Fig. 5 - Distance of closest approach as a function of initial impact parameter for various values of the reduced kinetic energy K, for the Lennard-Jones potential.

Fig. 6 - Distance of closest approach for the two-well potential. The light dashed curves give the loci of turning points for the various types of rainbow and glory scattering.

Fig. 7 - Semiclassical deflection angle and phase shift for the two-well potential, at various values of the reduced kinetic energy. Dashed curves refer to the Lennard-Jones potential.

Fig. 8 - Topology of scattering for the Lennard-Jones potential.

Fig. 9 - Topology of scattering for the two-well potential. The inner orbiting curve, which extends from $K = 0.35$ to $K = 5.16$, was inadvertently left unlabelled.

Fig. 10 - Form factors for (a) rainbow scattering and (b) glory scattering, as defined in Tables II and III.

Fig. 11 - Plots of dimentionless parameters θ_r, $B^{1/3}\Delta\theta_r$, and $B^{-1/6}H_r$ for rainbow scattering (see Table II) versus reduced kinetic energy. The "outer" rainbow of Fig. 7 (which is identical to that for the Lennard-Jones potential) is labelled "0"; the "inner" negative and positive rainbows are labelled "-" and "+", respectively.

Fig. 12 - Dimensionless parameters $\Delta\theta_o$ and H_o for orbiting (see Table II) versus reduced kinetic energy. "Outside" and "Inside" refer to the two branches of the deflection function (see Fig. 7), with positive and negative slopes, respectively. Below K = 0.8 the curves refer to "van der Waals orbiting", and the dashed portion of the "Inside" curves applies to the Lennard-Jones potential. Above K = 0.8 the curves refer to "chemical orbiting" associated with the innter centrifugal barrier of Fig. 4. The dot-dashed portion of the "Outside" curves indicates the region excluded because the outer part of the chemical orbiting deflection function gives way to the van der Waals orbiting or rainbow scattering (see Fig. 7).

Fig. 13 - Dimensionless parameters $B^{1/2}\Delta\theta_g$ and H_g for glory scattering versus reduced kinetic energy (see Table II). Dashed curves refer to the Lennard-Jones potential, solid curves to the two-well potential.

Fig. 14 - Angular distributions corresponding to the deflection functions shown in Fig. 7. The ordinates of the K = 2 and K = 0.6 curves should be multiplied by factors of 25 and 250, respectively.

Fig. 15 - Dimensionless glory scattering phase shift, $B^{-1/2}\eta_g$, and relative amplitude, $B^{9/20}U$, versus reduced kinetic energy. Dashed curves refer to the Lennard-Jones potential; solid curves to the two-well potential.

FOOTNOTES

1. D. Beck, E.F. Greene, and J. Ross, J. Chem. Phys. 37, 2895 (1962).

2. M. Ackermann, E.F. Greene, A. L. Moursund and J. Ross, Ninth Symposium on Combustion, p. 669 (Academic Press, New York, 1963).

3. E. Gersing, E. Hundhausen, and H. Pauly, Z. Physik 171, 349 (1963).

4. K.R. Wilson, J.H. Birely, R.R. Herm, and D.R. Herschbach, experiments to be described in a forthcoming University of California Radiation Laboratory Report.

5. See, for example, R.M. Eisberg and C.E. Porter, Rev. Mod. Phys. 33, 190 (1961).

6. J.O. Hirschfelder, C. F. Curtiss, and R.B. Bird, Molecular Theory of Gases and Liquids (Wiley, New York, 1954).

7. D. Beck, J. Chem. Phys. 37, 2884 (1962).

8. L. Pauling, Nature of the Chemical Bond (Cornell University Press, Ithaca, New York, 3rd Ed., 1960), p. 260.

9. E.W. Rothe, P.K. Rol, and R.B. Bernstein, Phys. Rev. 130, 2333 (1963).

10. G. Herzberg, Spectra of Diatomic Molecules (D. Van Nostrand Co., New York, 1950), p. 534.

11. L. Brewer and E. Brackett, Chem. Rev. 61, 425 (1961).

12. W. Klemperer and S.A. Rice, J. Chem. Phys. 26, 618; 27, 573 (1957).

13. Honig, Mandel, Stitch, and Townes, Phys. Rev. 96, 629 (1954).

14. See, for example, Eyring, Walter, and Kimball, Quantum Chemistry (Wiley, New York, 1944), p. 191.

15. E.B. Wilson and J.B. Howard, J. Chem. Phys. 4, 260 (1936); S.M. Ferigle and A. Weber, Am. J. Phys. 21, 102 (1953).

16. For discussions of vibrational and rotational energy transfer in collisions, see Herzfeld and Litovitz, Absorption and Dispersion of Ultrasonic Waves (Academic Press, New York, 1959), or Cottrell and McCoubrey, Molecular Energy Transfer in Gases (Butterworths, London, 1961).

17. Glasstone, Laidler, and Eyring, The Theory of Rate Processes (McGraw-Hill Book Co., New York, 1941).

18. Herschbach, Johnston, Pitzer, and Powell, J. Chem. Phys. 25, 736 (1956).

19. H.S. Johnston, Adv. Chem. Phys. 3, 131 (1960).

20. Reference 6; also, E. A. Mason and J. O. Hirschfelder, J. Chem. Phys. 26, 756 (1957).

21. J.L. Magee, J. Chem. Phys. 8, 677 (1940); J.L. Magee and T. Ri, J. Chem. Phys. 9, 638 (1941).

22. K. Takayanagi, Prog. Th. Phys. Japan 8, 497 (1952); 9, 578 (1953).

23. J.P. Toennies, Disc. Faraday Soc. 33, 96 (1962).

24. Bernstein, Dalgarno, Massey, and Percival, Proc. Roy. Soc. A274, 427 (1963).

25. E.A. Mason and L. Monchick, J. Chem. Phys. 35, 1676 (1961); 36, 1622 (1962).

26. F.T. Wall, L.A. Hiller, and J. Mazur, J. Chem. Phys. 29, 255 (1958); 35, 1284 (1961); N.C. Blais and D.L. Bunker, J. Chem. Phys. 37, 2713 (1962); 39, 315 (1963).

27. R.J. Cross and D.R. Herschbach, "Classical Scattering of Atoms by Diatomic Rigid Rotor Molecules," UCRL-10706 (February, 1963), p.53.

28. K.W. Ford and J.A. Wheeler, Ann. Phys. 7, 259 (1959).

29. H.S.W. Massey and C.B.O. Mohr, Proc. Roy. Soc. (London) A144, 188 (1934).

30. R.B. Bernstein and K.H. Kramer, J. Chem. Phys. 38, 2507 (1963).

31. R.B. Bernstein, J. Chem. Phys. 34, 361 (1961); 37, 1880 (1962); 38, 2599 (1963).

32. See, for example, T. Wu and T. Ohmura, Quantum Theory of Scattering (Prentice-Hall, Inc., Englewood Cliffs, New Jersey, 1962).

33. E.R. Rothe, P.K. Rol, S.M. Trujillo, and R.H. Neynaber, Phys. Rev. 128, 659 (1962); P.K. Rol and E.W. Rothe, Phys. Rev. Letters 9, 494 (1962); E.W. Rothe, R.H. Neynaber, B.W. Scott, S.M. Trujillo, and P.K. Rol, J. Chem. Phys. 39, 493 (1963).